Journal of Sound and Vibration 329 (2010) 833–847

Contents lists available at ScienceDirect

Journal of Sound and Vibration

journal homepage: www.elsevier.com/locate/jsvi

Vibration and critical speeds of composite-ring disks for data storage

Kyo-Nam Koo [a,*], George A. Lesieutre [b]

[a] Department of Aerospace Engineering, University of Ulsan, Ulsan 680-749, Republic of Korea
[b] Department of Aerospace Engineering, Pennsylvania State University, University Park, PA 16802, USA

ARTICLE INFO

Article history:
Received 3 April 2009
Received in revised form
19 August 2009
Accepted 27 September 2009
Handling Editor: L.G. Tham

ABSTRACT

A new concept for data storage disks is proposed to increase operating speed with minimum changes in the geometry and design of conventional data storage disks. The disk—named a composite-ring disk—is composed of a storage material inside and a thin composite ring outside. Stress distributions are found for the rotating disk composed of two annular disks, of which the inside is made of isotropic material and the outside is made of orthotropic material. The dynamic equation for a composite-ring disk in rotation is formulated to calculate its natural frequencies and critical speeds. For the solution of transverse vibration, a rotational symmetry condition is applied in the circumferential direction and a finite element interpolation with Hermite polynomials is performed in the radial direction. The results show that reinforcing a disk at the rim increases critical speeds drastically, and can cause buckling in mode (0,0) which occurs above the lowest critical speed.

1. Introduction

Optical and magnetic data storage devices read and write data on rotating disks. Rotation speed is a significant factor limiting the data transfer rate. The RAMAC unveiled in 1956 was the first commercial computer that used a hard disk drive [1]. The memory capacity of the system disk was only 4.8 megabytes (MB) in 50 disks 24 inches in diameter. Around 250 MB of data can now be stored on a disk 3.5 inches in diameter with recent PMR (perpendicular magnetic recording) technology [2]. According to Hitachi Ltd. [3], PMR technology will allow a recording density of up to one terabit (Tb) per square inch. In the optical data storage industry, HDDS (holographic digital data storage) technology, which stores data in three-dimensional space, is under intensive investigation for practical use. HDDS has high potential due to fast transfer rates of up to hundreds of MB/s and storage densities of up to one terabyte (TB) of data per 120 mm disk.

The higher the data transfer rate required by computers, the faster a storage disk should rotate. However, dynamic instability due to high rotation speed can cause errors in reading and writing data. Dimensional stability against thermal loading is another significant factor for a storage disk with high data density. Koo [4,5] showed that the use of composite materials in rotating disks can increase critical speeds dramatically. Since fiber-reinforced composite materials have a high specific modulus as well as a very low coefficient of thermal expansion (CTE) in the fiber direction, fiber-reinforced composite materials can be regarded as suitable for data storage disks, as well as the rotating machinery discussed in previous work, to enhance both vibrational and thermal stability.

* Corresponding author. Tel.: +82 52 259 1261; fax: +82 52 259 1682.
E-mail addresses: knkoo@mail.ulsan.ac.kr (K.-N. Koo), g-lesieutre@psu.edu (G.A. Lesieutre).

0022-460X/$ - see front matter © 2009 Elsevier Ltd. All rights reserved.
doi:10.1016/j.jsv.2009.09.040

Nomenclature

a, b	outer and inner radii of disk
c	radius of disk at the material interface
C	coefficient for in-plane displacements
$\mathbf{C}$	stiffness matrix
D_{ij}	bending stiffness
E, G	elastic and shear moduli
h	thickness of disk
H_i	Hermite polynomials
J	Jacobian
$\mathbf{K}$	stiffness matrix
m	number of nodal circles
$\mathbf{M}$	mass matrix
n	number of nodal diameters
$\overline{N}_r, \overline{N}_\theta, \overline{N}_{r\theta}$	in-plane force per length
r	radial coordinate
r_e	length of an element in radial direction
Δr	radial width of composite ring
R	function of radius
t	time
T	kinetic energy
u	in-plane displacement of disk
U	strain energy
w	transverse displacement of disk
$\mathbf{w}$	nodal displacement vector in finite element equation
ε, γ	normal and shear strains
θ	tangential coordinate in rotating coordinate
κ	curvature of the mid-plane
μ	modulus ratio
ν	Poisson's ratio
ξ	normal coordinate in a mater element $(-1 \le \xi \le 1)$
ρ	mass density of a disk
σ, τ	normal and shear stresses
ϕ	tangential coordinate in inertial coordinate
ψ	rotation angle at node
ω	angular frequency
Ω	rotating speed of disk
$\frac{\partial}{\partial r}, \frac{\partial}{\partial \theta}, \frac{\partial}{\partial t}$	partial derivatives
$\tilde{(\cdot)}$	in-plane quantity related with centrifugal inertia force
$\dot{(\cdot)}$	time derivative

Subscripts

1, 2	fiber and transverse direction of composite material
i, o	inner and outer disks
r, θ	radial and circumferential directions

Superscripts

b, f	backward and forward traveling waves
(e)	finite element
T	transpose of vector or matrix

However, all data storage disks must be fabricated with those materials which possess the optical or magnetic characteristics to record data. For instance, 120 mm diameter CDs and DVDs consist of lead-in area ($\varnothing$ 46–50 mm), program area ($\varnothing$ 50–116 mm), and lead-out area ($\varnothing$ 116–117 mm). Since the recording surface must be transparent, the application of composite materials is limited to the opposite surface and may have a high manufacturing cost.

Instead of using composite materials in the recording area of data storage disks, a new disk design proposed in this paper uses a composite ring to reinforce the rim of the disk with fibers along its hoop direction as shown in Fig. 1. The disk will be called a composite-ring disk hereafter. The in-plane stresses acting on the composite-ring disk due to rotation are found in order to study the effects of reinforcement on its dynamic characteristics. The dynamic equation for the composite-ring disk in rotation is formulated to calculate the natural frequencies and critical speeds. For the solution of transverse vibration, a rotational symmetric condition is applied in the circumferential direction and a finite element

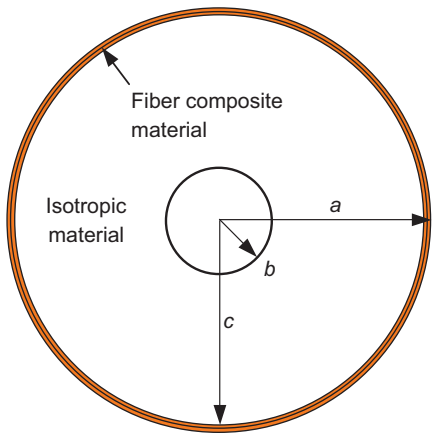

Fig. 1. Concept of composite-ring disk; $\Delta r = a - c$: radius of reinforcement.

interpolation with Hermite polynomials is performed in the radial direction. The numerical results show that the new concept proposed in this paper is very effective in enhancing the dynamic stability of the data storage disk, thus enabling higher rotation speeds and data transfer rates.

2. Governing equations and finite element formulation

2.1. Strain and kinetic energies of a rotating composite-ring disk

A composite-ring disk is composed of an isotropic inner disk for recording and a composite-ring with reinforcing fibers in the circumferential direction at its rim as shown in Fig. 1. Since isotropic materials may be considered a subset of orthotropic materials, the stress–strain relations for polar orthotropic materials in the plane stress state are used for both materials:

$$\begin{Bmatrix} \sigma_r \\ \sigma_\theta \\ \tau_{r\theta} \end{Bmatrix} = \begin{bmatrix} \dfrac{E_r}{1-\nu_{r\theta}\nu_{\theta r}} & \dfrac{\nu_{r\theta}E_\theta}{1-\nu_{r\theta}\nu_{\theta r}} & 0 \\ \dfrac{\nu_{\theta r}E_r}{1-\nu_{r\theta}\nu_{\theta r}} & \dfrac{E_\theta}{1-\nu_{r\theta}\nu_{\theta r}} & 0 \\ 0 & 0 & G_{r\theta} \end{bmatrix} \begin{Bmatrix} \varepsilon_r \\ \varepsilon_\theta \\ \gamma_{r\theta} \end{Bmatrix} \quad \text{or} \quad \boldsymbol{\sigma} = \mathbf{C}\boldsymbol{\varepsilon}, \tag{1}$$

where $\boldsymbol{\sigma}$ and $\boldsymbol{\varepsilon}$ is the stress and strain vectors, respectively; $\mathbf{C}$ the stiffness matrix; and $\nu_{r\theta}/E_r = \nu_{\theta r}/E_\theta$.

Two polar coordinate systems are introduced to describe the motion of a rotating disk with thickness h as shown in Fig. 2. The (r,θ)-coordinate system rotates at a constant speed Ω fixed to the disk and the (r,ϕ)-coordinate system does not rotate, instead remaining fixed in inertial space.

Since the disk dealt in this paper behaves as a thin elastic plate, it is assumed that:

- the transverse shear deformation and rotary inertia may be neglected;
- the in-plane forces induced by rotation is assumed to be unaffected by the transverse motion; and
- the effect of in-plane vibration is neglected.

The strain energy of a rotating thin disk consists of the bending strain energy U_B and the strain energy associated with the membrane stresses due to rotation U_Ω:

$$U = U_B + U_\Omega. \tag{2}$$

The bending strain energy of an orthotropic disk can be expressed in the (r,θ)-coordinate system by

$$U_B = \frac{1}{2}\int_b^a \int_0^{2\pi} \boldsymbol{\kappa}^{\mathrm{T}}\mathbf{D}\boldsymbol{\kappa} r \,\mathrm{d}r\,\mathrm{d}\theta, \tag{3}$$

where $\boldsymbol{\kappa}$ is the vector for the curvature of the mid-plane and $\mathbf{D}$ the bending stiffness matrix. The vector $\boldsymbol{\kappa}$ and the matrix $\mathbf{D}$ are defined as

$$\boldsymbol{\kappa} = \begin{Bmatrix} \kappa_r \\ \kappa_\theta \\ \kappa_{r\theta} \end{Bmatrix}, \mathbf{D} = \begin{bmatrix} D_r & D_{r\theta} & 0 \\ D_{r\theta} & D_\theta & 0 \\ 0 & 0 & D_k \end{bmatrix}, \tag{4}$$

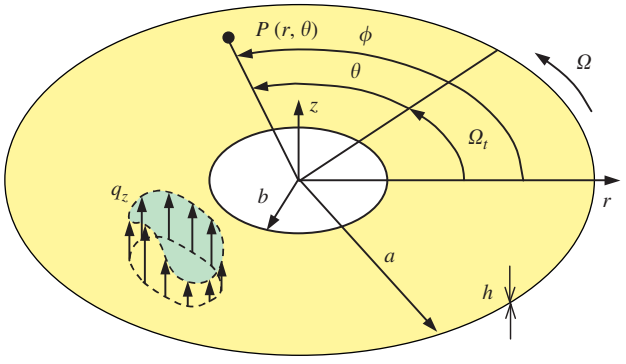

Fig. 2. Coordinates and geometry of rotating disk.

where the elements of $\boldsymbol{\kappa}$ and $\mathbf{D}$ are

$$\kappa_r = \frac{\partial^2 w}{\partial r^2}, \quad \kappa_\theta = \frac{\partial w}{r\partial r} + \frac{\partial w}{r^2 \partial \theta^2}, \quad \kappa_{r\theta} = 2\frac{\partial}{\partial r}\left(\frac{\partial w}{r\partial \theta}\right), \tag{5a}$$

$$D_r = \frac{E_r h^3}{12(1 - \nu_{r\theta}\nu_{\theta r})}, \quad D_\theta = \frac{E_\theta h^3}{12(1 - \nu_{r\theta}\nu_{\theta r})}, \quad D_{r\theta} = \nu_{r\theta} D_\theta, \quad D_k = \frac{G_{r\theta} h^3}{12}. \tag{5b}$$

The strain energy associated with the membrane stresses caused by rotation is given by

$$U_\Omega = \frac{1}{2}\int_b^a \int_0^{2\pi} \left\{ \overline{N}_r \left(\frac{\partial w}{\partial r}\right)^2 + \overline{N}_\theta \left(\frac{\partial w}{r\partial \theta}\right)^2 \right\} r \, \mathrm{d}r \, \mathrm{d}\theta, \tag{6}$$

where $\overline{N}_r$ and $\overline{N}_\theta$ are the in-plane force per unit length produced by centrifugal inertia force.

Since the natural frequencies are computed in the rotating coordinate system and then the natural frequencies in the inertial coordinate system are obtained from Eq. (31), the kinetic energy associated only with the transverse vibration of a disk is considered:

$$T = \frac{1}{2}\int_b^a \int_0^{2\pi} \rho h \left(\frac{\partial w}{\partial t}\right)^2 r \, \mathrm{d}r \, \mathrm{d}\theta. \tag{7}$$

If we include the kinetic energy associated with disk rotation in Eq. (7), the frequencies in the inertial coordinate system are directly obtained without Eq. (31).

2.2. In-plane loading due to rotation

The force resultants $\overline{N}_r$ and $\overline{N}_\theta$ can be determined from the equation of motion in the r-direction:

$$-\frac{\partial}{\partial r}(r\overline{N}_r) - \frac{\partial \overline{N}_{r\theta}}{\partial \theta} + \overline{N}_\theta = r(\rho h r \Omega^2), \tag{8}$$

where $\partial \overline{N}_{r\theta}/\partial\theta$ vanishes for an axisymmetric problem.

The strain–displacement relations under in-plane loading due to rotation are written by

$$\overline{\varepsilon}_r = \frac{\partial \overline{u}_r}{\partial r}, \quad \overline{\varepsilon}_\theta = \frac{1}{r}\left(\overline{u}_r + \frac{\partial \overline{u}_\theta}{\partial \theta}\right), \quad \overline{\gamma}_{r\theta} = r\frac{\partial}{\partial r}\left(\frac{\overline{u}_\theta}{r}\right) + \frac{\partial \overline{u}_r}{r\partial \theta}. \tag{9}$$

Integrating Eq. (1) through the thickness after substituting Eq. (9) into Eq. (1) with $\partial(\,)/\partial\theta = 0$ for the axisymmetric situation, $\overline{N}_r$ and $\overline{N}_\theta$ are expressed by

$$\overline{N}_r = K_r \frac{\mathrm{d}\overline{u}_r}{\mathrm{d}r} + \nu_{r\theta} K_\theta \frac{\overline{u}_r}{r}, \quad \overline{N}_\theta = \nu_{\theta r} K_r \frac{\mathrm{d}\overline{u}_r}{\mathrm{d}r} + K_\theta \frac{\overline{u}_r}{r}, \tag{10}$$

where $K_r = E_r h/(1 - \nu_{r\theta}\nu_{\theta r})$ and $K_\theta = E_\theta h/(1 - \nu_{r\theta}\nu_{\theta r})$.

Substituting $\overline{N}_r$ and $\overline{N}_\theta$ obtained by using Eq. (10) into Eq. (8) yields a differential equation for the radial displacement of points on the mid-plane:

$$r^2 \frac{\mathrm{d}^2 \overline{u}_r}{\mathrm{d}r^2} + r\frac{\mathrm{d}\overline{u}_r}{\mathrm{d}r} - \mu^2 \overline{u}_r = -\frac{\rho h \Omega^2 r^3}{K_r}, \tag{11}$$

where $\mu^2 = E_\theta/E_r$; $\mu^2 = 1$ and $K_r = K = Eh/(1 - \nu^2)$ for isotropic materials. The solutions to Eq. (11) for inner isotropic and outer orthotropic disks, $\overline{u}_{ri}$ and $\overline{u}_{ro}$, respectively, are obtained as

$$\overline{u}_{ri}(r) = C_{1i} r + C_{2i} r^{-1} - \frac{\rho_i h \Omega^2 r^3}{8K}, \tag{12a}$$

$$\overline{u}_{ro}(r) = C_{1o} r^{\mu} + C_{2o} r^{-\mu} - \frac{\rho_o h \Omega^2 r^3}{(9 - \mu^2)K_r}. \tag{12b}$$

The coefficients C_{1i}, C_{2i}, C_{1o}, and C_{2o} in Eq. (12) are determined from boundary conditions. The typical data storage disk is fixed at the inner radius b and free at the outer radius a and its boundary conditions are given by:

$$\overline{u}_{ri}(b) = 0, \tag{13a}$$

$$\overline{N}_{ro}(a) = 0. \tag{13b}$$

The displacement and the force resultant in the radial direction should be continuous at the radius of the material interface, $c(b<c<a)$:

$$\overline{u}_{ri}(c) = \overline{u}_{ro}(c), \quad \overline{N}_{ri}(c) = \overline{N}_{ro}(c). \tag{14}$$

Using Eqs. (10) and (12), the conditions in Eqs. (13) and (14) are expressed as follows:

$$bC_{1i} + b^{-1}C_{2i} = \frac{\rho_i h\Omega^2 b^3}{8K}, \tag{15a}$$

$$\mu(1+\mu\nu_{r\theta})a^{\mu-1}C_{1o} - \mu(1-\mu\nu_{r\theta})a^{-\mu-1}C_{2o} = \frac{(3+\mu^2\nu_{r\theta})\rho_o h\Omega^2 a^3}{(9-\mu^2)K_r}, \tag{15b}$$

$$cC_{1i} + c^{-1}C_{2i} - c^{\mu}C_{1o} - c^{-\mu}C_{2o} = \frac{\rho_i h\Omega^2 c^3}{8K} - \frac{\rho_o h\Omega^2 c^3}{(9-\mu^2)K_r}, \tag{15c}$$

$$\begin{aligned}&(1+\nu)KC_{1i} - (1-\nu)Kc^{-2}C_{2i} - \mu(1+\mu\nu_{r\theta})K_r c^{\mu-1}C_{1o} + \mu(1-\mu\nu_{r\theta})c^{-\mu-1}C_{2o}\\ &= \frac{(3+\nu)\rho_i h\Omega^2 c^2}{8} - \frac{(3+\mu^2\nu_{r\theta})\rho_o h\Omega^2 c^2}{9-\mu^2}.\end{aligned} \tag{15d}$$

These simultaneous equations give the coefficients C_{1i}, C_{2i}, C_{1o}, and C_{2o}, with which the displacements and force resultants can be expressed.

2.3. Finite element interpolation for transverse vibration

Since the transverse displacement $w(r,\theta)$ of a disk in vibration is rotationally symmetric, it can be assumed to be

$$w(r,\theta,t) = R(r)\cos(n\theta). \tag{16}$$

Therefore, a finite element formulation is required only in the radial direction as done by Kirkhope and Wilson [6]. The finite element interpolation expresses the displacement in a linear combination of shape functions:

$$R(r) = \sum_{i=1}^{4} H_i w_i = \mathbf{H}^{\mathrm{T}}\mathbf{w}^{(e)}, \tag{17}$$

where w_i are the nodal displacements and H_i are the Hermite interpolation functions given in Appendix A. For an element length r_e in the radial direction, they are given by

$$\mathbf{w}^{(e)} = \{w_1 \;\; \psi_1 \;\; w_2 \;\; \psi_2\}^{\mathrm{T}}, \tag{18}$$

$$\mathbf{H} = \{H_1 \;\; H_2 \;\; H_3 \;\; H_4\}^{\mathrm{T}}. \tag{19}$$

The strain and kinetic energies of an element can be discretized as

$$U_B^{(e)} = \frac{1}{2}\mathbf{w}^{(e)\mathrm{T}}(l\pi\int_{r_e}\mathbf{B}^{\mathrm{T}}\mathbf{D}\mathbf{B}r\,\mathrm{d}r)\mathbf{w}^{(e)}, \tag{20}$$

$$U_\Omega^{(e)} = \frac{1}{2}\mathbf{w}^{(e)\mathrm{T}}\left[l\pi\int_{r_e}\left(r\overline{N}_r\frac{\mathrm{d}\mathbf{H}}{\mathrm{d}r}\frac{\mathrm{d}\mathbf{H}^{\mathrm{T}}}{\mathrm{d}r} + \frac{n^2}{r}\overline{N}_\theta\mathbf{H}\mathbf{H}^{\mathrm{T}}\right)\mathrm{d}r\right]\mathbf{w}^{(e)\mathrm{T}}, \tag{21}$$

$$T^{(e)} = \frac{1}{2}\dot{\mathbf{w}}^{(e)\mathrm{T}}\left(l\pi\int_{r_e}\rho h\mathbf{H}\mathbf{H}^{\mathrm{T}}r\,\mathrm{d}r\right)\dot{\mathbf{w}}^{(e)}, \tag{22}$$

where

$$l = \begin{cases}2 & \text{for } n=0\\ 1 & \text{for } n\geq 1\end{cases}, \tag{23}$$

$$\mathbf{B} = \mathbf{b}\mathbf{H}^{\mathrm{T}} \quad \text{and} \quad \mathbf{b} = \left\{\left(\frac{\mathrm{d}^2}{\mathrm{d}r^2}\right) \;\; \left(\frac{\mathrm{d}}{r\,\mathrm{d}r} - \frac{n^2}{r^2}\right) \;\; 2n\left(\frac{\mathrm{d}}{r\,\mathrm{d}r} + \frac{1}{r^2}\right)\right\}^{\mathrm{T}}. \tag{24}$$

The Lagrange equation with these expressions for the discretized energies then yields the equations of motion for an element:

$$\mathbf{M}^{(e)}\ddot{\mathbf{w}}^{(e)} + (\mathbf{K}_B^{(e)} + \Omega^2\mathbf{K}_\Omega^{(e)})\mathbf{w}^{(e)} = \mathbf{0}^{(e)}, \tag{25}$$

where the element stiffness and mass matrices are defined by

$$\mathbf{K}_B^{(e)} = l\pi\int_{r_e}\mathbf{B}^{\mathrm{T}}\mathbf{D}\mathbf{B}r\,\mathrm{d}r, \tag{26}$$

$$\mathbf{K}_{\Omega}^{(e)} = l\pi \int_{r_e} \left(r\overline{N}_r \frac{\mathrm{d}\mathbf{H}}{\mathrm{d}r} \frac{\mathrm{d}\mathbf{H}^{\mathrm{T}}}{\mathrm{d}r} + \frac{n^2}{r} \overline{N}_{\theta} \mathbf{H}\mathbf{H}^{\mathrm{T}} \right) \mathrm{d}r, \tag{27}$$

$$\mathbf{M}^{(e)} = l\pi \int_{r_e} \rho h \mathbf{H}\mathbf{H}^{\mathrm{T}} r \, \mathrm{d}r. \tag{28}$$

The integration in Eqs. (26)–(28) is performed in normal coordinate by using the Gauss quadrature. The elements of $\mathbf{K}_{B}^{(e)}$, $\mathbf{K}_{\Omega}^{(e)}$, and $\mathbf{M}^{(e)}$ are given in Appendix A.

The in-plane loads $\overline{N}_r$ and $\overline{N}_{\theta}$ at the Gauss points can be obtained by interpolating linearly in an element as follows:

$$\overline{N}_r(r) = \frac{\overline{N}_{r(k+1)} - \overline{N}_{r(k)}}{r_e}(r - r_k) + \overline{N}_{r(k)}, \tag{29a}$$

$$\overline{N}_{\theta}(r) = \frac{\overline{N}_{\theta(k+1)} - \overline{N}_{\theta(k)}}{r_e}(r - r_k) + \overline{N}_{\theta(k)} \tag{29b}$$

where a starting node in the k-th element is regarded as k.

Table 1
Material properties of polycarbonate, GFRP, and CFRP.

Material	E_1 (GPa)	E_2 (GPa)	G_{12} (GPa)	ν_{12}	ρ (kg/m^3)
Polycarbonate	2.2	2.2	0.797	0.38	1220
GFRP(E-glass/epoxy)	38.6	8.27	4.14	0.26	1800
CFRP(T300/N5208)	181.0	10.3	7.17	0.28	1600

Table 2
Natural frequencies (Hz) of CFRP-ring disk with $\Delta r = 1$.

Mode		(0,0)	(0,1)	(0,2)	(0,3)	(0,4)	(0,5)
0 rev/min	Present	148.5	127.1	196.6	492.7	941.4	1481.9
	NASTRAN	148.4	126.9	196.4	492.8	942.1	1482.7
10,000 rev/min	Present	191.0	222.9	367.9	666.8	1095.9	1609.9
	NASTRAN	190.8	222.8	367.8	666.8	1096.0	1609.9

Table 3
Variation of natural frequencies of non-rotating disks with radius width of GFRP ring.

Δr (mm)	Natural frequencies of each mode (Hz)					
	(0,0)	(0,1)	(0,2)	(0,3)	(0,4)	(0,5)
0.0	131.7	125.0	152.3	273.5	468.1	718.0
1.0	134.0	123.5	161.2	329.5	602.7	964.6
2.0	136.0	122.3	169.0	372.3	696.4	1122.0
3.0	137.7	121.3	176.0	407.4	769.9	1241.7
4.0	139.3	120.5	182.4	437.2	831.4	1340.9
5.0	140.9	119.8	188.2	463.3	884.7	1427.1

Table 4
Variation of natural frequencies of non-rotating disks with radius width of CFRP ring.

Δr (mm)	Natural frequencies of each mode (Hz)					
	(0,0)	(0,1)	(0,2)	(0,3)	(0,4)	(0,5)
0.0	131.7	125.0	152.3	273.5	468.1	718.0
1.0	148.5	127.1	196.6	492.7	941.4	1481.9
2.0	157.5	128.2	228.1	624.1	1173.5	1752.0
3.0	163.4	128.8	253.0	722.8	1330.1	1909.6
4.0	168.0	129.3	273.8	803.4	1451.4	2029.0
5.0	171.8	129.8	291.6	872.4	1554.8	2133.6

After assembling all the elements and assuming the motion to be harmonic, the natural frequencies in the rotating coordinate system (r,θ) can be computed from the following eigenvalue problem:

$$(\mathbf{K}_{\mathcal{B}} + \Omega^2\mathbf{K}_{\Omega} - \omega^2\mathbf{M})\mathbf{w} = \mathbf{0}. \tag{30}$$

A natural frequency in the rotating coordinates (r,θ) is split into two natural frequencies in the inertial coordinates (r,ϕ) as

$$\omega^f_{mn} = \omega_{mn} + n\Omega, \tag{31a}$$

$$\omega^b_{mn} = \omega_{mn} - n\Omega, \tag{31b}$$

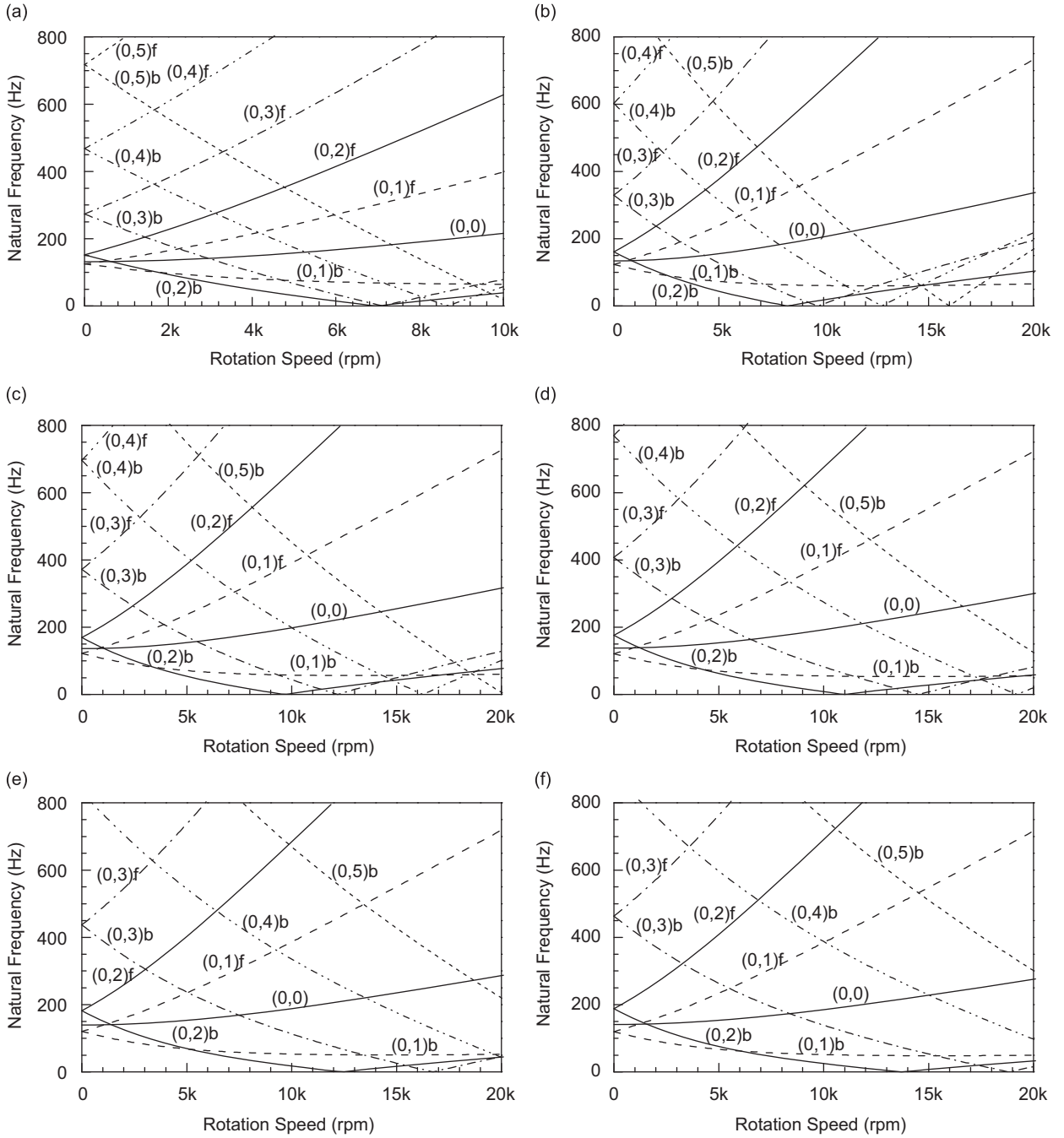

Fig. 3. Frequency–speed diagram of GFRP-ring disk: (a) $\Delta r = 0$ mm; (b) $\Delta r = 1$ mm; (c) $\Delta r = 2$ mm; (d) $\Delta r = 3$ mm; (e) $\Delta r = 4$ mm; and (f) $\Delta r = 5$ mm.

where ω_{mn}^{f} is the natural frequency of the forward traveling wave and ω_{mn}^{b} the natural frequency of the backward traveling wave. The subscripts m and n in Eq. (31) denote the number of nodal circles and diameters, respectively.

A critical speed can be determined when the backward frequency ω_{mn}^{b} vanishes. In this situation, the propagation speed of the backward traveling wave in the rotating frame is equal to the disk rotation speed. This means that the backward traveling wave is stationary in the inertial frame at the critical speed. A stationary transverse load applied to the disk at critical speeds, without any damping mechanism, would cause the amplitude of transverse motion to be unbounded.

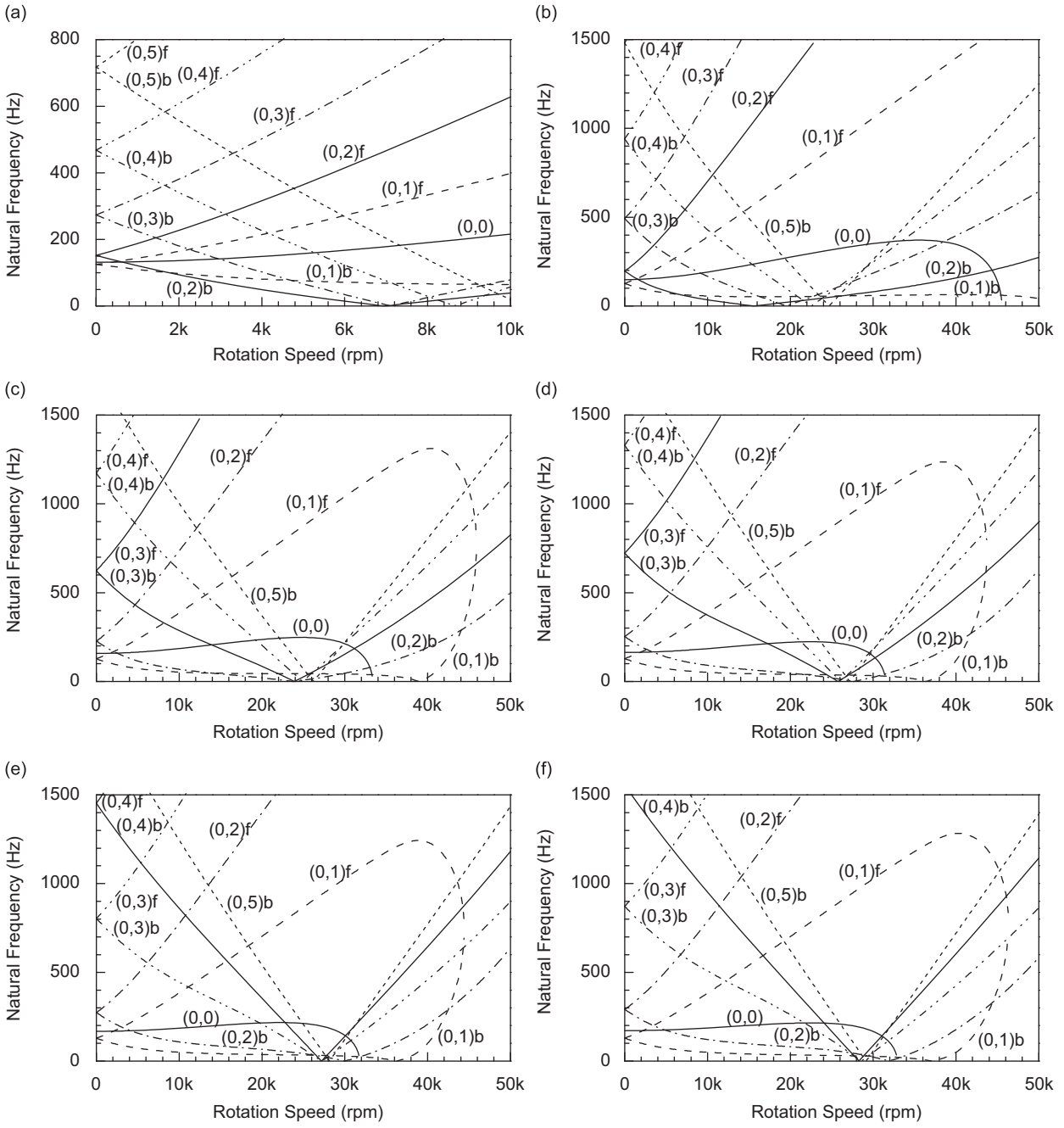

Fig. 4. Frequency–speed diagram of CFRP-ring disk: (a) $\Delta r = 0$ mm; (b) $\Delta r = 1$ mm; (c) $\Delta r = 2$ mm; (d) $\Delta r = 3$ mm; (e) $\Delta r = 4$ mm; and (f) $\Delta r = 5$ mm.

3. Results and discussion

The proposed concept for data storage disks is applied to an optical disk with typical dimensions:

$$b = 15\,\text{mm}, \quad a = 60\,\text{mm}, \quad h = 1.2\,\text{mm}$$

where b is the inner radius along which the disk is fixed and a the outer radius along which the disk is free. Instead of using composite materials in the whole disk, the disk is reinforced only at the rim by fibers along the hoop direction as shown in Fig. 1. The radial width of the composite ring is defined as $\Delta r = a - c$, where c is the radius to the interface between isotropic and composite materials.

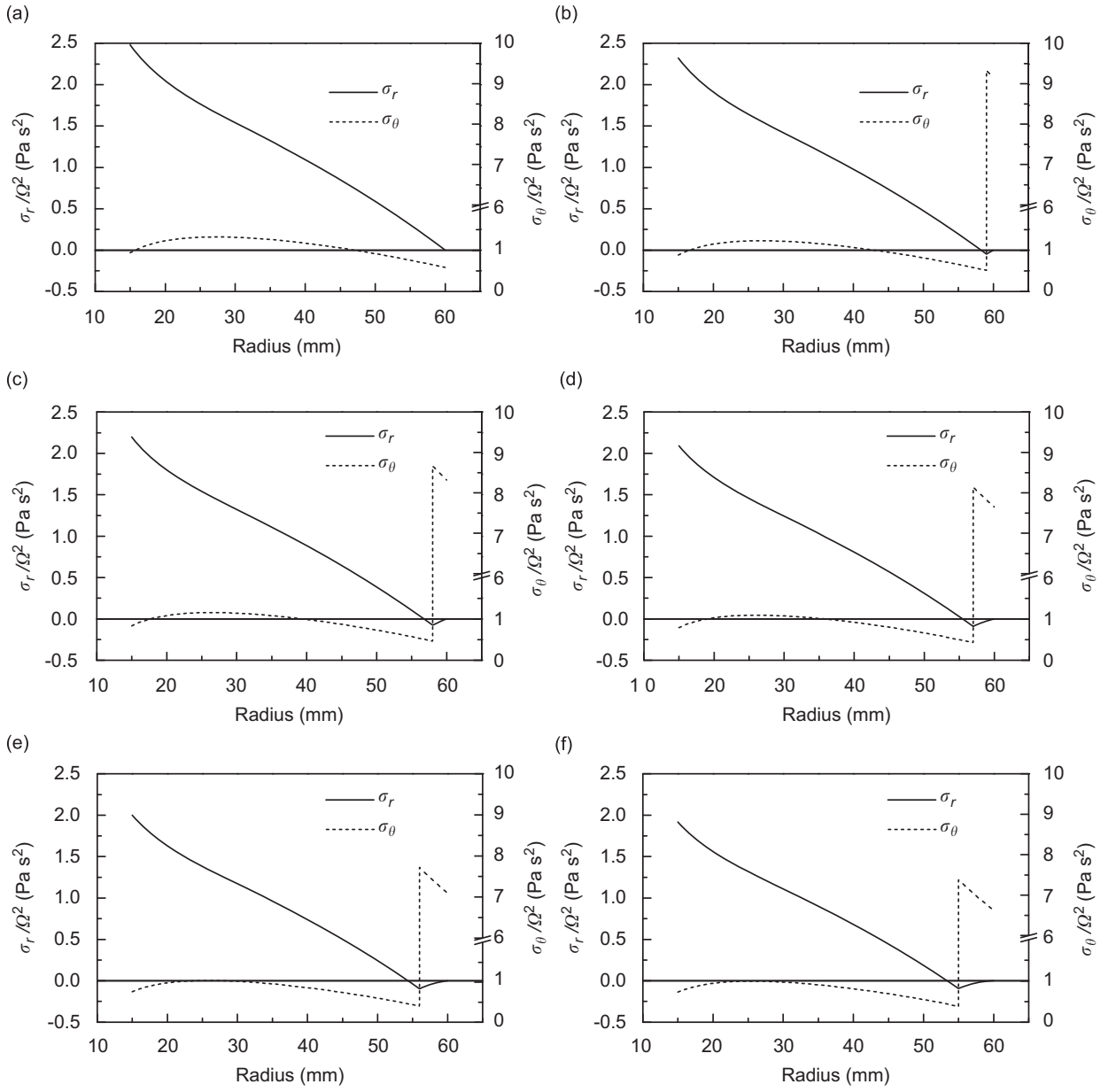

Fig. 5. Radial stress σ_r/Ω^2 and circumferential stress σ_θ/Ω^2 of GFRP-ring disk: (a) $\Delta r = 0$ mm; (b) $\Delta r = 1$ mm; (c) $\Delta r = 2$ mm; (d) $\Delta r = 3$ mm; (e) $\Delta r = 4$ mm; and (f) $\Delta r = 5$ mm.

3.1. Disks consisting of practical materials

A disk consists of a PC (polycarbonate) inner disk for recording and a fiber-reinforced composite ring at the rim for reinforcement. Material properties used in this study are displayed in Table 1. E-glass/epoxy and T300/N5208 were chosen in this study as the typical GFRP (glass fiber reinforced plastic) and CFRP (carbon fiber reinforced plastic), respectively. The material constants for composite ring should be assigned in the following way: $E_r = E_2$, $E_\theta = E_1$, $G_{r\theta} = G_{21} = G_{12}$, $\nu_{r\theta} = \nu_{21}$. About 45 finite elements with an equal length with which the solution was sufficiently converged are used in the radial direction for all cases in this study.

In order to validate the present method, in Table 2 are displayed the natural frequencies of the CFRP-ring disk with $\Delta r = 1$ mm in the rotating coordinate system. In MSC/NASTRAN analysis, the disk was modeled with 45 elements along the radial direction and 144 elements along the circumferential direction. The normal mode analysis of a rotating disk in MSC/NASTRAN should utilize a solution sequence SOL 106 [7]. The results of MSC/NASTRAN in Table 2 do not have the effects of transverse shear and rotary inertia. It is displayed in Table 2 that the present results are in very good agreement with the finite element results.

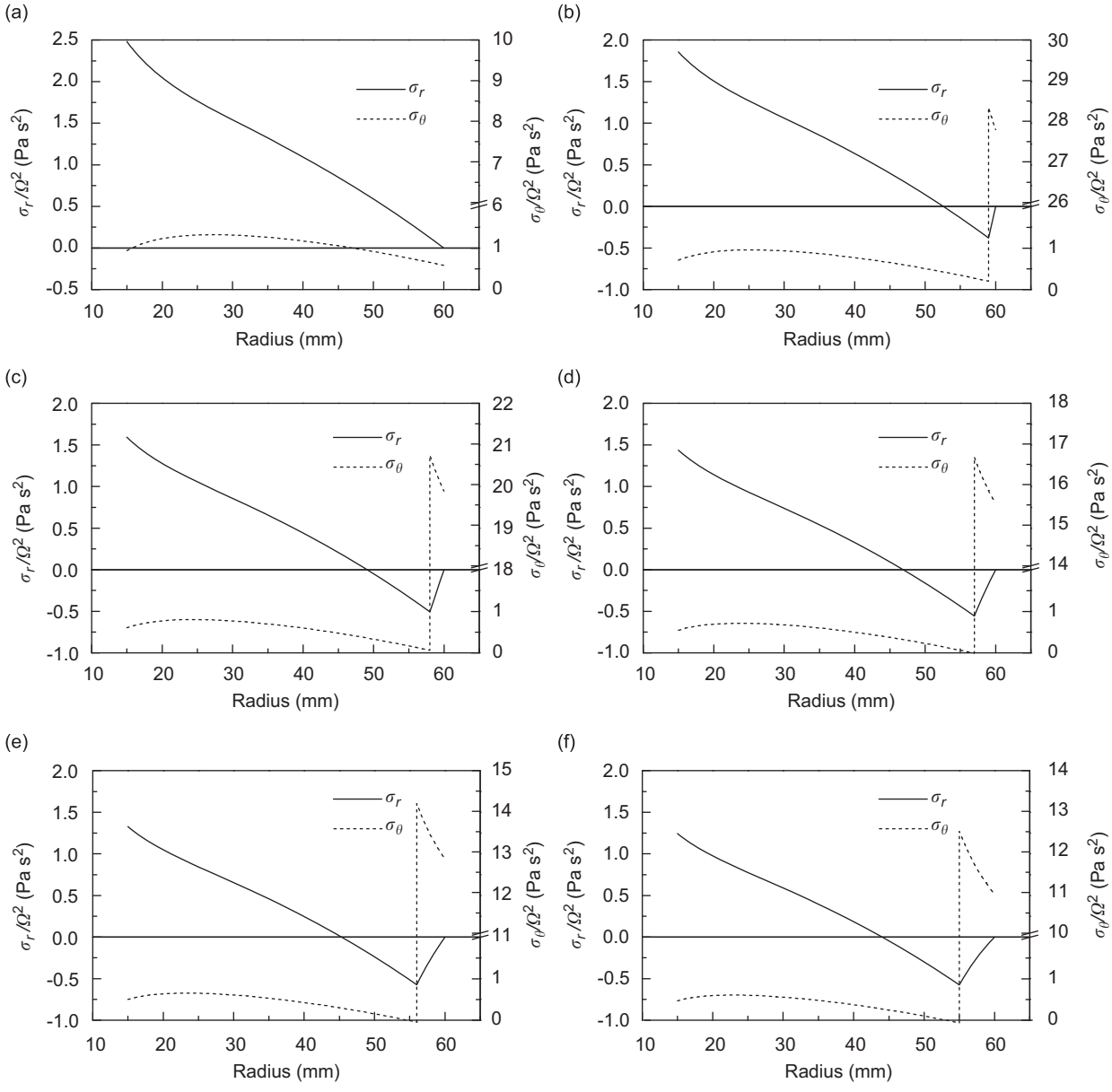

Fig. 6. Radial stress σ_r/Ω^2 and circumferential stress σ_θ/Ω^2 of CFRP-ring disk: (a) $\Delta r = 0$ mm; (b) $\Delta r = 1$ mm; (c) $\Delta r = 2$ mm; (d) $\Delta r = 3$ mm; (e) $\Delta r = 4$ mm; and (f) $\Delta r = 5$ mm.

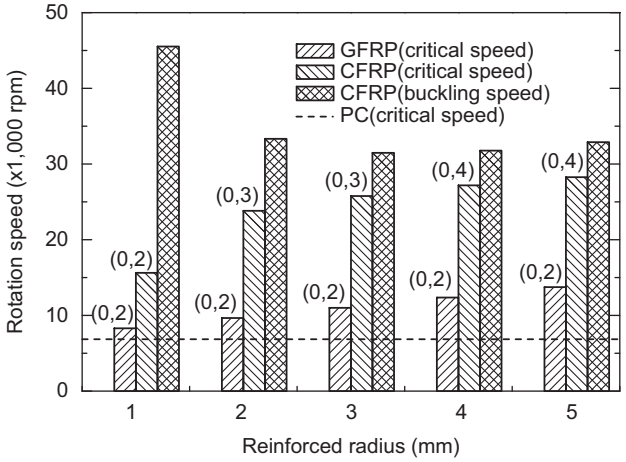

Fig. 7. Critical and buckling speeds of PC and composite-ring disks.

Tables 3 and 4 display how the natural frequencies of a non-rotating disk change as the radial width of the GFRP and CFRP rings changes. The mode (m, n) has m nodal circles and n nodal diameters. It is observed in Table 3 that the GFRP ring increases the natural frequencies of all modes except for mode (0,1). This implies that the GFRP ring may make an improvement of the dynamic stability of the rotating disk by the GFRP ring, but not much. Noticeably, the 5 mm GFRP ring decreases the natural frequency of mode (0,1) by 4 percent. This is because an increment in the bending stiffness for mode (0,1) is very small but the mass effect for mode (0,1) relatively increases much more. As displayed in Table 4, the CFRP ring increases the natural frequencies of all modes. The increment in the natural frequency due to the CFRP ring is very small in mode (0,1) compared with that in the other modes. This is due to the fact that the effect of stiffening in bending is very small in mode (0,1) because the disk bends mostly in the polycarbonate with little deformation in the CFRP ring. The natural frequency of mode (0,1) increases by 4 percent for the width $\Delta r = 5$ mm whereas that of mode (0,2) increases by 91 percent. In general, the use of a composite ring with high modulus can drastically increase the critical speed since the critical mode in rotating disks is typically mode (0,2) or (0,3).

Figs. 3 and 4 show the natural frequencies of rotating disks with a GFRP ring and a CFRP ring, respectively. In those figures, $(m, n)f$ and $(m, n)b$ refer to the forward and backward traveling modes in the inertial frame, respectively. Fig. 3(a) shows that the lowest critical speed of the original CD (corresponding to $\Delta r = 0$) is about 7060 rev/min in mode (0,2). Fig. 3 shows that the GFRP ring can effectively increase the critical speed. In particular, the 5 mm GFRP ring increases the critical speed by 65 percent in comparison with the original polycarbonate disk. It is observed in Fig. 4(b) that even the 1 mm CFRP ring increases the critical speed by 2.2 times compared with the polycarbonate disk.

Note that the frequency of mode (0,0) becomes zero at a certain rotation speed around 45,528 rev/min for $\Delta r = 1$ mm. This phenomenon corresponds to buckling since mode (0,0) does not have a mode split. A buckling speed can be defined as a speed at which the natural frequency in a rotating coordinate system is zero. Therefore, a bucking speed can be distinguished from a critical speed by checking the natural frequency in the rotating coordinate system instead of in the inertia coordinate system. Buckling occurs only in the CFRP-ring disks but not in the GFRP-ring disks. This is because the high stiffness of the CFRP ring in the fiber direction acts as a constraint to induce a compressive stress field in the polycarbonate area. Figs. 5 and 6 where the unit of Ω is rad/s illustrate the radial and circumferential stresses (σ_r and σ_θ), induced by rotation, of the GFRP-ring and CFRP-ring disks, respectively. The isotropic disk has only the tensile stress in the radial direction. Only tensile stress is induced in the isotropic disk by rotation whereas the compressive stress acts in the interface area of the composite-ring disk. This is due to the fact that the composite ring prevents the inside disk from extending. It is observed in the figures that there is a discontinuity of circumferential stress at the interface of the two materials. The low level of the compressive stress is apparent in a small area for the GFRP-ring disk as shown in Fig. 5. However, as shown in Fig. 6, the level of the compressive stress in the CFRP-ring disk is much higher and acts over a much wider area. This suggests that buckling may be a concern in a rotating disk with a composite ring having a very high modulus.

Fig. 7 summarizes the critical and buckling speeds of the disks addressed in this paper. The number on each bar refers to the critical mode. The dynamic stability of an isotropic disk can be dramatically enhanced by reinforcing its rim with composite material. Even though the CFRP-ring disk is susceptible to buckling, it has a buckling speed higher than the lowest critical speed. Another observation is that the CFRP-ring disk with $\Delta r = 5$ mm does not have the lowest buckling speed though it has the highest level and widest area of compressive stress among the disks. This is due to the fact that buckling is dependent on the characteristic dimension of a structure or radius for a disk in addition to the stress level.

Figs. 8 and 9 compares the mode shapes of the PC and CFRP-ring disks at various speeds, respectively. There seems to be little difference between the mode shapes of the PC disk at non-rotating and critical speeds, as shown in Fig. 8. This implies

that the mode shape of a non-rotating isotropic disk can be used to determine the critical speed of the rotating disk. Fig. 9 shows that the mode shape of the composite-ring disk is more dependent on rotating speed than that of the PC disk. And the mode shape at the buckling speed is dramatically different from the others. Therefore, the functions used for a series solution should be carefully selected in the buckling analysis of a rotating composite-ring disk.

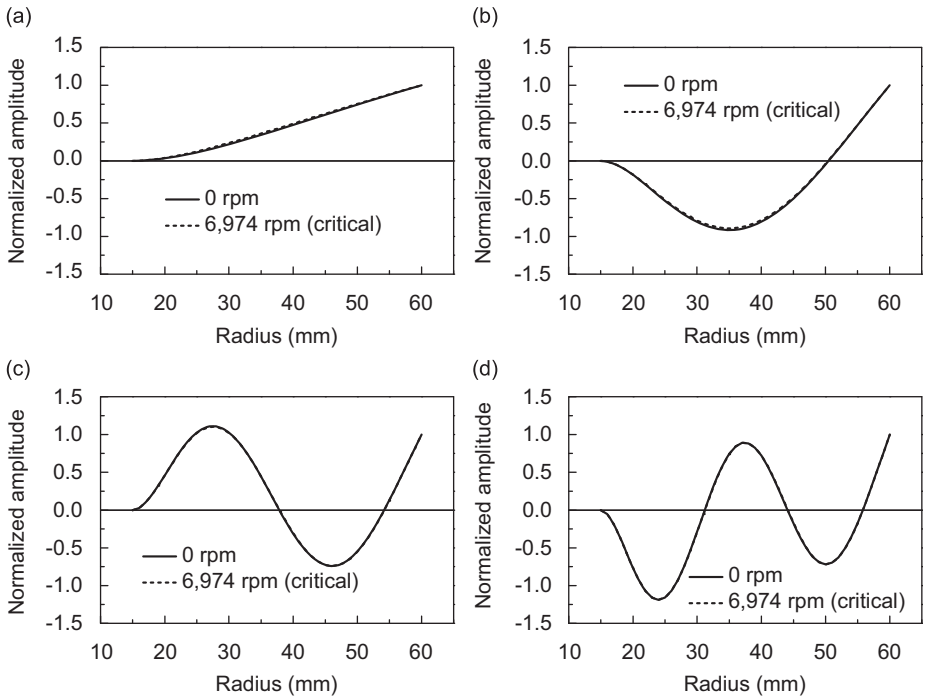

Fig. 8. Mode shapes of PC disks: (a) mode (0,0); (b) mode (0,1); (c) mode (0,2); and (d) mode (0,3).

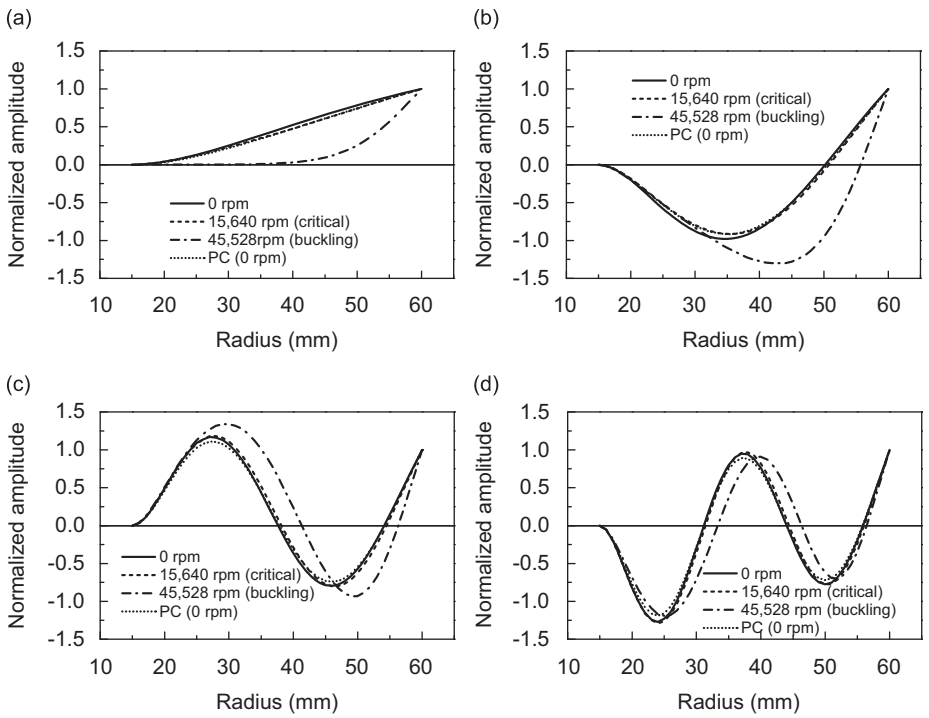

Fig. 9. Mode shapes for PC and CFRP-ring disks with $\Delta r = 1$ mm: (a) mode (0,0); (b) mode (0,1); (c) mode (0,2); and (d) mode (0,3).

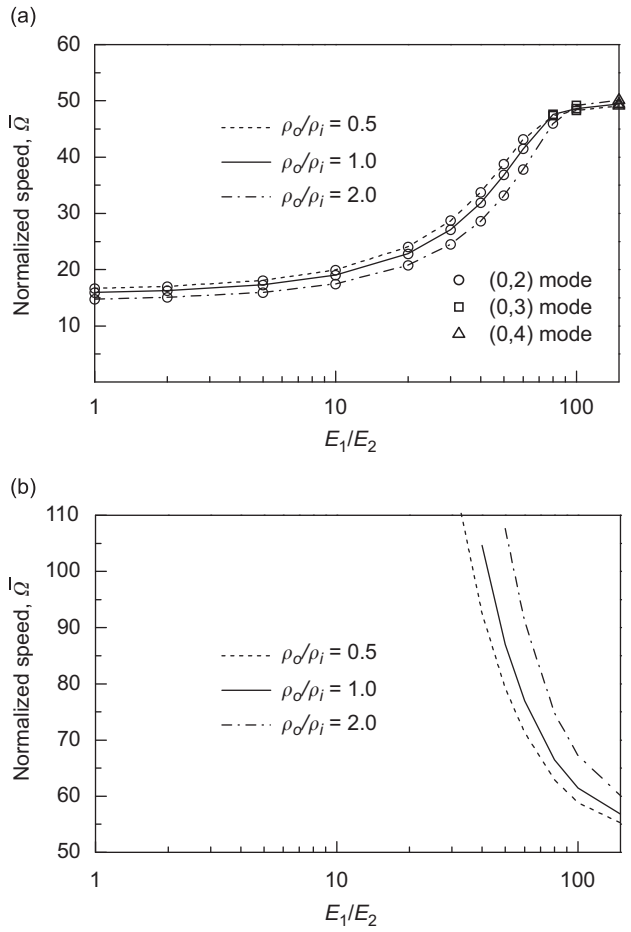

Fig. 10. Effects of modulus and density ratios on critical and buckling speeds of composite-ring disks: (a) critical speeds and (b) buckling speeds.

3.2. Effects of modulus and density ratios

In order to gain more general insight into the dynamic behavior of rotating composite-ring disks, the effect of the modulus ratio of composite material and the density ratio between isotropic and composite materials on the critical and buckling speeds was studied. The modulus ratio E_1/E_2 is defined as a ratio of elastic moduli in the fiber and transverse directions. The density ratio ρ_o/ρ_i is the ratio of the density of the composite ring, ρ_o to the density of the inner disk material, ρ_i. The other geometric parameters and material constants used in this study are given by

$$b/a = 0.25, \quad \Delta r/a = 0.025, \quad a/h = 400, \quad G_{12}/E_2 = 0.5, \quad \nu_{12} = 0.25.$$

For $E_1/E_2 = 1$, which corresponds to an isotropic material, G_{12}/E_2 is changed to 0.4 for material consistency.

Fig. 10 shows the critical and buckling speeds of composite-ring disks with various modulus and density ratios. The critical speed increases as the modulus ratio increases for all density ratios. The critical speed increases very little over the range up to $E_1/E_2 = 80$ and the critical mode is shifted from mode (0,2) to a higher mode. The critical speed is also lower for higher density ratios. This is because a higher density ratio reduces the natural frequency. As seen earlier, Fig. 9(b) indicates that the high stiffness of the composite ring in the hoop direction prevents the disk from extending, so the disk is more susceptible to buckling. Although the high modulus ratio adversely affects the buckling, the buckling speed is still higher than the critical speed in the practical range of the modulus ratio for all density ratios. A higher density ratio also increases the buckling speed for a given modulus ratio. This is due to the fact that the more mass the composite ring has, the more tensile stress is induced by centrifugal force.

Fig. 11 illustrates the variation in stresses with the change of the modulus and density ratio of the composite-ring disk. As the modulus ratio increases, the radial stress level decreases and its compressive field becomes wider. This is due to the fact that the high stiffness of the composite ring prevents the inner disk from extending. This reduces the buckling speed for the disk with a high stiffness ratio. Finally, the stresses in the inner disk of the composite-ring disk with high modulus ratio are less dependent on density ratio than in the composite-ring disk with low modulus ratio.

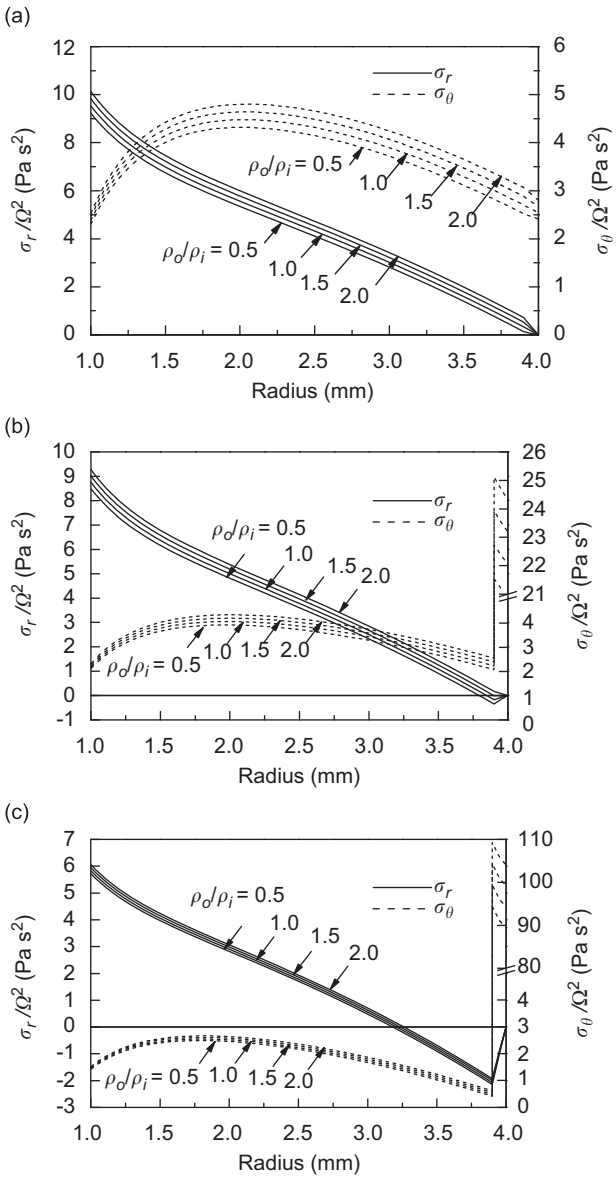

Fig. 11. Effects of modulus and density ratios on stresses of composite-ring disks: (a) $E_1/E_2 = 1$; (b) $E_1/E_2 = 10$; and (c) $E_1/E_2 = 100$.

4. Conclusions

Rotating disks may suffer from dynamic instability so that their operating speed is limited by the critical speed. A demand for higher data transfer rates in computers requires higher rotational speed in optical and magnetic data storage disks. The results in this paper show that data storage disks reinforced by an outer composite ring have increased critical speeds. The benefit and effectiveness of the composite-ring disk was verified by numerical studies. The dynamic equation for a rotating composite-ring disk was formulated to calculate natural frequencies and critical speed. A rotational symmetric condition was applied in the circumferential direction and a finite element interpolation was performed in the radial direction for the solution of transverse vibration.

The reinforcement of an isotropic disk with a composite ring was shown to increase the critical speed drastically. Although buckling may occur in composite-ring disks, the buckling speed is greater than the critical speed for composite-ring disks with practical moduli and density ratios. A composite ring can be very effective in increasing the critical speed of data storage disks with no significant changes in shape or mass.

Appendix A

Eqs. (26)–(28) are evaluated in normal coordinate $\xi(-1\leq\xi\leq1)$ instead of in global coordinate $r(r_k\leq r\leq r_{k+1})$ where r_k and r_{k+1} denote the coordinates of the inner and outer end nodes of the k-th element.

The Hermite polynomials in the normal coordinate $\xi(-1\leq\xi\leq1)$ are defined by

$$H_1(\xi)=\tfrac{1}{4}(2-3\xi+\xi^3), \tag{A.1}$$

$$H_2(\xi)=\frac{r_e}{8}(1-\xi+\xi^2+\xi^3), \tag{A.2}$$

$$H_3(\xi)=\tfrac{1}{4}(2+3\xi-\xi^3), \tag{A.3}$$

$$H_4(\xi)=\frac{r_e}{8}(-1-\xi+\xi^2+\xi^3). \tag{A.4}$$

For the stiffness and mass matrices, we have

$$\begin{aligned}K_{Bij}^{(e)}=l\pi\int_{r_e}\Bigg[&D_r\left(\frac{\mathrm{d}^2H_i}{J^2\,\mathrm{d}\xi^2}\right)\left(\frac{\mathrm{d}^2H_j}{J^2\,\mathrm{d}\xi^2}\right)+D_{r\theta}\left(\frac{\mathrm{d}^2H_i}{J^2\,\mathrm{d}\xi^2}\right)\left(\frac{\mathrm{d}H_i}{\xi J\,\mathrm{d}\xi}-\frac{n^2H_j}{\xi^2}\right)+D_{r\theta}\left(\frac{\mathrm{d}H_i}{\xi J\,\mathrm{d}\xi}-\frac{n^2H_i}{\xi^2}\right)\left(\frac{\mathrm{d}^2H_j}{J^2\,\mathrm{d}\xi^2}\right)\\&+D_\theta\left(\frac{\mathrm{d}H_i}{\xi J\,\mathrm{d}\xi}-\frac{n^2H_i}{\xi^2}\right)\left(\frac{\mathrm{d}H_j}{\xi J\,\mathrm{d}\xi}-\frac{n^2H_j}{\xi^2}\right)+4n^2D_k\left(\frac{\mathrm{d}H_i}{\xi J\,\mathrm{d}\xi}-\frac{H_i}{\xi^2}\right)\left(\frac{\mathrm{d}H_j}{\xi J\,\mathrm{d}\xi}-\frac{H_j}{\xi^2}\right)\Bigg]\xi|J|\,\mathrm{d}\xi,\end{aligned} \tag{A.5}$$

$$K_{\Omega ij}^{(e)}=l\pi\int_{-1}^{1}\left[\xi\overline{N}_r(\xi)\frac{\mathrm{d}H_i(\xi)}{J\,\mathrm{d}\xi}\frac{\mathrm{d}H_j(\xi)}{J\,\mathrm{d}\xi}+\frac{n^2}{\xi^2}\overline{N}_\theta(\xi)H_i(\xi)H_j(\xi)\right]\xi|J|\,\mathrm{d}\xi, \tag{A.6}$$

$$M_{ij}^{(e)}=l\pi\int_{-1}^{1}\rho hH_i(\xi)H_j(\xi)\xi|J|\,\mathrm{d}\xi, \tag{A.7}$$

where $J=\mathrm{d}r/\mathrm{d}\xi=r_e/2$.

References

[1] 〈http://www-03.ibm.com/ibm/history/exhibits/storage/storage_350.html〉 (accessed 1 September 2008).
[2] 〈http://www.pcworld.com/article/id,128400-page,1/article.html〉 (accessed 1 September 2008).
[3] 〈http://www.hitachi.com/New/cnews/071015a.html〉 (accessed 1 September 2008).
[4] K.-N. Koo, Vibration analysis and critical speeds of polar orthotropic annular disks in rotation, *Composite Structures* 76 (2006) 67–72. doi:10.1016/j.compstruct.2006.06.010.
[5] K.-N. Koo, Mechanical vibration and critical speeds of rotating composite laminate disks, *Microsystem Technologies* 14 (2008) 799–807. doi:10.1007/s00542-007-0555-2.
[6] J. Kirkhope, G.J. Wilson, Vibration and stress analysis of thin rotating discs using annular finite elements, *Journal of Sound and Vibration* 44 (1976) 461–474.
[7] D.N. Herting, *MSC/NASTRAN Advanced Dynamics Analysis User's Guide*, The MacNeal-Schwendler Corporation, CA, 1997.